NASA TECHNICAL NOTE

NASA TN D-8126

NASA TN D-8126

CYCLIC DEBONDING OF UNIDIRECTIONAL COMPOSITE BONDED TO ALUMINUM SHEET FOR CONSTANT-AMPLITUDE LOADING

George L. Roderick, Richard A. Everett, Jr., and John H. Crews, Jr.

Langley Research Center
Hampton, Va. 23665

NATIONAL AERONAUTICS AND SPACE ADMINISTRATION • WASHINGTON, D. C. • JANUARY 1976

1. Report No. NASA TN D-8126
2. Government Accession No.
3. Recipient's Catalog No.

4. Title and Subtitle
CYCLIC DEBONDING OF UNIDIRECTIONAL COMPOSITE BONDED TO ALUMINUM SHEET FOR CONSTANT-AMPLITUDE LOADING

5. Report Date
January 1976
6. Performing Organization Code

7. Author(s)
George L. Roderick, Richard A. Everett, Jr., and John H. Crews, Jr.

8. Performing Organization Report No.
L-10480
10. Work Unit No.
505-02-31-01

9. Performing Organization Name and Address
NASA Langley Research Center
Hampton, Va. 23665

11. Contract or Grant No.
13. Type of Report and Period Covered
Technical Note

12. Sponsoring Agency Name and Address
National Aeronautics and Space Administration
Washington, D.C. 20546

14. Sponsoring Agency Code

15. Supplementary Notes
George L. Roderick and Richard A. Everett, Jr.: Langley Directorate, U.S. Army Air Mobility R&D Laboratory.
John H. Crews, Jr.: Langley Research Center.

16. Abstract

Cyclic debonding rates were measured during constant-amplitude loading of specimens made of graphite/epoxy bonded to aluminum and S-glass/epoxy bonded to aluminum. Both room-temperature and elevated-temperature curing adhesives were used. Debonding was monitored with a photoelastic coating technique. The debonding rates were compared with three expressions for strain-energy release rate calculated in terms of the maximum stress, stress range, or a combination of the two.

The debonding rates were influenced by both adherend thickness and the cyclic stress ratio. For a given value of maximum stress, lower stress ratios and thicker specimens produced faster debonding. Microscopic examination of the debonded surfaces showed different failure mechanisms both for identical adherends bonded with different adhesive and, indeed, even for different adherends bonded with identical adhesives.

The expressions for strain-energy release rate correlated the data for different specimen thicknesses and stress ratios quite well for each material system, but the form of the best correlating expression varied among material systems. Consequently, empirical correlating expressions applicable to one material system may not be appropriate for another system, and caution should be exercised in drawing parallels between different material systems without supporting test data.

17. Key Words (Suggested by Author(s))
Fatigue tests
Fatigue (materials)
Adhesive bonding
Composite materials
Structural engineering

18. Distribution Statement
Unclassified – Unlimited
Subject Category 39

19. Security Classif. (of this report) Unclassified
20. Security Classif. (of this page) Unclassified
21. No. of Pages 34
22. Price* $3.75

*For sale by the National Technical Information Service, Springfield, Virginia 22161

CYCLIC DEBONDING OF UNIDIRECTIONAL COMPOSITE BONDED TO ALUMINUM SHEET FOR CONSTANT-AMPLITUDE LOADING

George L. Roderick,* Richard A. Everett, Jr.,*
and John H. Crews, Jr.
Langley Research Center

SUMMARY

Cyclic debonding rates were measured during constant-amplitude loading of specimens made of graphite/epoxy bonded to aluminum and S-glass/epoxy bonded to aluminum. Both room-temperature and elevated-temperature curing adhesives were used. Debonding was monitored with a photoelastic coating technique. The debonding rates were compared with three expressions for strain-energy release rate calculated in terms of the maximum stress, stress range, or a combination of the two.

The debonding rates were influenced by both adherend thickness and the cyclic stress ratio. For a given value of maximum stress, lower stress ratios and thicker specimens produced faster debonding. Microscopic examination of the debonded surfaces showed different failure mechanisms both for identical adherends bonded with different adhesive and, indeed, even for different adherends bonded with identical adhesives.

The expressions for strain-energy release rate correlated the data for different specimen thicknesses and stress ratios quite well for each material system, but the form of the best correlating expression varied among material systems. Consequently, empirical correlating expressions applicable to one material system may not be appropriate for another system, and caution should be exercised in drawing parallels between different material systems without supporting test data.

INTRODUCTION

Adhesive bonds are widely used to join structural components. Such joints produce milder stress concentrations than do mechanically fastened joints. Adhesively bonded joints are particularly advantageous for composite materials because stress concentrations, such as bolt holes, can significantly reduce the static strength of such materials.

Bonds can also be used to join layers of different materials to make one new, improved material. For example, hybrid bonded systems of metal and composite

*Langley Directorate, U.S. Army Air Mobility R&D Laboratory.

layers are stronger for equal weight and stiffness than metals alone (ref. 1). Indeed, composites themselves derive their high efficiency from a collection of bonded constituent materials. However, under cyclic loading the bond is often the weakest point in a bonded system. Once started, cyclic debonding usually continues progressively (ref. 2) and compromises the integrity of the bonded system. Consequently, when debonding is detected in a structure, its rate of propagation is crucial in determining the component reliability and in establishing inspection intervals. Unfortunately, very little is known about cyclic debonding, and a designer has no rationale to predict debonding rates. A concept which can be used as the basis of such a rationale is presented in this paper and is used to analyze cyclic debonding data.

This paper presents an analysis for constant-amplitude cyclic debonding of simple laminated specimens made of aluminum alloy sheets bonded to a unidirectional graphite or fiberglass composite. The analysis is based on correlations of the observed debonding rates with calculated rates of strain-energy release that accompanies cyclic debonding. Because the debonding rates are intimately related to the debonding failure modes, typical failure surfaces are examined for each of the three material systems studied.

SYMBOLS

The units for the physical quantities defined in this paper are given in the International System of Units (SI) (ref. 3). The measurements and calculations were made in the U.S. Customary Units.

a	debond length, m
da/dN	debond-propagation rate, m/cycle
c,n	curve-fit parameters
E	Young's modulus, Pa
G	strain-energy release rate, J/m
L	length, m
N	number of cycles
P	applied load, N
R	ratio of minimum-to-maximum applied stress

RT	room temperature
r	residual from least-squares curve fit, m/cycle
S	stress in region A of composite sheet, Pa
t	thickness, m
ΔT	change in temperature between cure and test temperatures, K
U	strain energy, J
V	volume, m^3
w	specimen width, m
x,y	Cartesian coordinates, m
α	thermal expansion coefficient, K^{-1}
δ	deflection, m
ϵ	strain
σ	stress, Pa
ϕ	strain-energy density, J/m^3

Subscripts:

A	region A
B	region B
C	region C
max	maximum value of stress
min	minimum value of stress

range range of stress

max·range product of maximum stress and range of stress

1 aluminum

2 composite

EXPERIMENTAL PROCEDURE

Specimens and Loading

Figure 1 shows the specimen configuration used in the present study. The specimen consisted of two aluminum alloy sheets adhesively bonded to a unidirectional composite core. (See table I for the material properties.) Three combinations of materials were tested and will be referred to as material systems I, II, and III, as shown in the following table:

Material system	Composite	Adhesive		
		Type	Thickness, mm	Cure temperature, K
I	Graphite/epoxy	EA-927R[a]	0.13	294 (RT)
II	Graphite/epoxy	AF-126[b]	.13	394
III	S-glass/epoxy	AF-126[b]	.13	394

[a] In EA-927R, the scrim cloth is a woven cloth with fibers parallel and perpendicular to the longitudinal axis of the specimen.

[b] In AF-126 the scrim cloth is a mat cloth with randomly oriented fibers.

The specimen was designed for rapid debond initiation. A severe stress concentration was introduced in the form of the abrupt change of section. Under cyclic loading, debonding started readily at this stress concentration.

The experimental program included tests for ranges of material thicknesses, maximum applied stresses, and stress ratios. (See tables II, III, and IV.) For all the tests, the cyclic frequency was 10 Hz.

Measurement of Debonding Rates

A photoelastic technique was used to monitor the debond front. Figure 2 shows the location of the photoelastic coatings on the specimen and typical isochromatic fringes.

Photoelastic coatings were bonded to the aluminum surfaces of the specimen; the surfaces were viewed through a polarizer and quarter-wave plate. Under load, isochromatic fringes developed at a debond front as a result of the high strain gradient in that vicinity. The test specimens were photographed at specified intervals throughout each test to record the position of the debond front.

STRAIN-ENERGY RELEASE RATE EQUATIONS

Basic Equation

Fatigue-crack-propagation rates in metals have been correlated with the strain-energy release rate G (ref. 4), where

$$G = P\frac{d\delta}{da} - \frac{dU}{da} \tag{1}$$

The term $P(d\delta/da)$ is the work done by the applied load as the crack extends, and dU/da is the change in the stored strain energy as the crack extends. Conceptually, because debond propagation in composites is analogous to fatigue-crack propagation in metals, such a correlation may also be valid for debond propagation. Accordingly, an expression for G was developed for the specimen configuration tested. This expression was determined using a one-dimensional elasticity analysis described in the following discussion.

To simplify the analysis, the specimen was divided into three regions of lengths L_A, L_B, and L_C (fig. 3). In regions A and C, only uniform strains in the x-direction were significant. Consequently, these regions could be analyzed by an elementary elasticity method. In contrast, region B had a complex strain distribution and could not be analyzed using elementary methods. But the strain distribution in region B, and consequently the length of region B, can be expected to remain constant as the debond extends. As will be shown, this constancy eliminated the need to calculate the strain distribution in region B.

An expression for $d\delta/da$ in equation (1) was derived from the increase in the end deflection of the specimen $d\delta$ caused by an increment of debonding da. Before an increment of debonding occurred, the end deflection was given by

$$\delta = \delta_A + \delta_B + \delta_C \tag{2}$$

and after debonding, by

$$\delta' = \delta'_A + \delta_B + \delta'_C \tag{3}$$

Because the strain distribution in region B was assumed to be the same before and after the region translated, the δ_B term did not change. To find $\Delta\delta$, equation (2) was subtracted from equation (3); thus,

$$\delta' - \delta = \Delta\delta = \delta'_A - \delta_A + \delta'_C - \delta_C \tag{4}$$

The deflections on the right side of equation (4) can be expressed in the general form

$$\delta = \epsilon L \tag{5}$$

Substitution of equation (5) into equation (4) yields:

$$\Delta\delta = \epsilon_A\left(L_A + \Delta a\right) - \epsilon_A L_A + \epsilon_C\left(L_C - \Delta a\right) - \epsilon_C L_C \tag{6}$$

$$\Delta\delta = \left(\epsilon_A - \epsilon_C\right)\Delta a \tag{7}$$

or

$$\lim_{\Delta a \to 0} \frac{\Delta\delta}{\Delta a} = \frac{d\delta}{da} = \epsilon_A - \epsilon_C \tag{8}$$

The expression for dU/da in equation (1) was derived by calculating the change of strain energy dU in the specimen resulting from an increment of debonding da. Employing the same reasoning used in the development of equation (4) allows the change in strain energy to be expressed as

$$U' - U = \Delta U = U'_A - U_A + U'_C - U_C \tag{9}$$

The strain energies on the right side of equation (9) can be expressed in the general form

$$U = \phi V \tag{10}$$

where ϕ is the strain-energy density and V is the volume of strained material. Substitution of equation (10) into equation (9) yields

$$\Delta U = \phi_{A,2} wt_2\left(L_A + \Delta a\right) - \phi_{A,2} wt_2 L_A + 2\phi_{C,1} wt_1\left(L_C - \Delta a\right) + \phi_{C,2} wt_2\left(L_C - \Delta a\right) - \left(2\phi_{C,1} wt_1 L_C + \phi_{C,2} wt_2 L_C\right) \tag{11}$$

$$\Delta U = w\left[\phi_{A,2} t_2 - \left(\phi_{C,2} t_2 + 2\phi_{C,1} t_1\right)\right]\Delta a \tag{12}$$

or

$$\lim_{\Delta a \to 0} \frac{\Delta U}{\Delta a} = \frac{dU}{da} = w\left[\phi_{A,2}t_2 - \left(\phi_{C,2}t_2 + 2\phi_{C,1}t_1\right)\right] \tag{13}$$

Substitution of equations (8) and (13) into equation (1) yields

$$G = P\left(\epsilon_A - \epsilon_C\right) - w\left[\phi_{A,2}t_2 - \left(\phi_{C,2}t_2 + 2\phi_{C,1}t_1\right)\right] \tag{14}$$

This equation is evaluated in the appendix in terms of applied stress, temperature change, material parameters, and specimen configuration and leads to

$$G = \frac{t_1 t_2 E_1 w}{E_2\left(2t_1E_1 + t_2E_2\right)}\left[S - \Delta T\left(\alpha_1 - \alpha_2\right)E_2\right]^2 \tag{15}$$

where the temperature change ΔT is the difference between the debond test temperature and the cure temperature of the adhesive.

Correlating Parameters

In the previous section the expression for the strain-energy release rate G was derived on the implicit assumption that the debond advanced while the specimen was subjected to a constant stress condition (constant applied stress and temperature). However, for cyclic debonding the relation between stress and debond extension is unknown. In fact, the debond may or may not extend throughout the entire stress cycle. Consequently, the actual value of G for cyclic debonding is unknown. However, the aforementioned analogy between cyclic debonding and crack propagation in metals suggests that the debonding process may be correlated with the maximum cyclic stress, the range of cyclic stress, or with a combination of the two. Consequently, three G parameters, each incorporating one of these three stress conditions, are developed herein and evaluated as correlation parameters.

To develop the G parameters for each of the three stress conditions, equation (15) was rewritten in the form

$$G = \frac{t_1 t_2 E_1 w}{E_2\left(2t_1E_1 + t_2E_2\right)}\sigma^2 \tag{16}$$

where

$$\sigma = S - \Delta T\left(\alpha_1 - \alpha_2\right)E_2$$

The G parameter for the maximum stress condition is derived by substituting σ_{max} for σ in equation (16), where

$$\sigma_{max} = S_{max} - \Delta T(\alpha_1 - \alpha_2)E_2 \tag{17}$$

Thus,

$$G_{max} = \frac{t_1 t_2 E_1 w}{E_2(2t_1E_1 + t_2E_2)}\left[S_{max} - \Delta T(\alpha_1 - \alpha_2)E_2\right]^2 \tag{18}$$

The G parameter for the stress range condition is derived by substituting $\Delta\sigma$ for σ in equation (16), where

$$\Delta\sigma = \sigma_{max} - \sigma_{min} = S_{max} - S_{min} \tag{19}$$

and

$$\sigma_{min} = S_{min} - \Delta T(\alpha_1 - \alpha_2)E_2 \tag{20}$$

Thus,

$$G_{range} = \frac{t_1 t_2 E_1 w}{E_2(2t_1E_1 + t_2E_2)}(S_{max} - S_{min})^2 \tag{21}$$

The G parameter for the combination condition is derived by substituting $\sigma_{max}\,\Delta\sigma$ for σ^2 in equation (16), where

$$\sigma_{max}\,\Delta\sigma = \left[S_{max} - \Delta T(\alpha_1 - \alpha_2)E_2\right](S_{max} - S_{min}) \tag{22}$$

Thus,

$$G_{max\cdot range} = \frac{t_1 t_2 E_1 w}{E_2(2t_1E_1 + t_2E_2)}\left[S_{max} - \Delta T(\alpha_1 - \alpha_2)E_2\right](S_{max} - S_{min}) \tag{23}$$

These three parameters are evaluated for specific materials in the next section.

RESULTS

Cyclic debonding tests were conducted for each of three material systems and are discussed in the following sequence: First, typical test results are discussed to illustrate the manner in which cyclic debonding progressed. Second, the topographies of the failure surfaces are analyzed. And third, the degree of correlation of the debonding data with each of the three strain-energy release parameters developed in the previous section is evaluated.

Typical Debonding Behavior

Figure 4 shows a typical variation of debond length with applied load cycles. In all cases debonding was initially nonlinear but became linear after the debond progressed a short distance.

For all three material systems, nonlinear debonding was confined to a region near the change of cross section of the specimens. This nonlinearity appears to be related to a transition of failure mode. In figure 4, for example, the light portion indicates failure within the adhesive and the darker portion indicates failure within the composite matrix. (Herein, matrix refers to the epoxy of the composite core.) Early transition of failure modes occurred in all three material systems.

Because nonlinear debonding occurred only during a small portion of each test, the correlation analysis presented herein considers only the significant linear portion.

Examination of Failure Surfaces

The possible failure modes for the specimens tested are numerous; failure can occur within the adhesive, at the interfaces between the aluminum and the composite, or in the composite itself at the fiber-matrix interfaces. Because these modes are intimately related to the debond-propagation rates, the failed surfaces of the specimens were examined with a scanning electron microscope. The results of these examinations are discussed in the following paragraphs.

Material system I (fig. 5).- When this system failed, adhesive remained on both the composite and the aluminum sheet. Within the adhesive, separation occurred at the interface between the scrim cloth and the adhesive. The figure shows a typical failure surface as viewed toward the debonded aluminum sheet. At the lowest magnification (fig. 5(a)), the failure surface appears to have a woven pattern. This pattern is the imprint of the scrim cloth on the adhesive. (After debonding the scrim cloth remained with the composite core.) Figure 5(b) shows these imprints at a higher magnification. At the highest magnification (fig. 5(c)), the individual scrim cloth fiber impressions exhibit striations. In this

system, the striations were difficult to find. However, striations were more apparent in the other material systems and will be discussed later.

Material system II (fig. 6).- This system failed primarily at the fiber-matrix interface, with some failure at the matrix-adhesive interface. After failure, the adhesive remained on the aluminum sheets. The figure shows a typical failure surface as viewed toward the debonded aluminum sheet. At the lowest magnification (fig. 6(a)), the smooth areas are fiber-matrix interface failure surfaces and the coarse areas are matrix-adhesive failures. On closer examination (fig. 6(b)), impressions of the graphite fibers can be seen on the smooth failure surface. At a higher magnification (fig. 6(c)), a graphite fiber impression exhibits striations. These were observed for the entire range of rates measured with this material. The striation spacings were in general agreement with the debonding rates.

Material system III (fig. 7).- In contrast to material system II, this system failed primarily at the matrix-adhesive interface, with some failure at the fiber-matrix interface. After failure, the adhesive remained on the aluminum sheet. The figure shows the failure surface as viewed toward the debonded aluminum sheet. At the lowest magnification (fig. 7(a)), the coarse area is the matrix-adhesive failure surface while the smooth area is the fiber-matrix failure surface. On closer examination (fig. 7(b)), S-glass fiber impressions can be seen on the smooth surface. At a higher magnification (fig. 7(c)), the S-glass fiber impressions exhibit striations. As in material system II, these striations were observed in all tests and generally correspond to the measured debonding rates.

Correlation of Debond-Propagation Rates

The measured debond-propagation rates da/dN and the corresponding S_{max} values, thicknesses, and stress ratios are shown in tables II, III, and IV. For each material system, at least two specimen thicknesses were tested for each of several stress ratios ranging from 0.10 to 0.48. In the following discussion, the propagation rates for each material system are plotted against the three previously developed strain-energy release rate parameters G_{max}, G_{range}, and $G_{max \cdot range}$ (eqs. (18), (21), and (23), respectively).

Material system I.- In figure 8(a) the rate data are plotted against S_{max}. The symbol shapes indicate different thicknesses and the symbol shadings indicate various ranges of stress ratio. The layering of these data indicates that for a given S_{max}, the thicker specimens debonded faster than the thinner ones, and the specimens tested at lower stress ratios debonded faster than specimens tested at higher stress ratios.

Figures 8(b), (c), and (d) show the data for material system I plotted against the three G parameters developed earlier. Figure 8(b) shows the data plotted against G_{max} (eq. (18)); figure 8(c) shows the data plotted against G_{range} (eq. (21)); and fig-

ure 8(d) shows the data plotted against $G_{max \cdot range}$ (eq. (23)). In all these figures, an equation of the form

$$\frac{da}{dN} = c(G)^n \tag{24}$$

was fit to the data using a least-squares fit. (In the least-squares method the arbitrary constants c and n are chosen to give the smallest error between values from eq. (24) and test values.) Mathematically, the goodness of fit is represented as the sum of the squares of the errors Σr^2 between the calculated values and the test values – the smaller Σr^2, the better the fit. Visually, the goodness of fit can be represented by confidence limits as discussed in reference 5. The 95-percent confidence limits are shown in the figures by solid lines – the closer these lines lie together, the better the correlation. The 95-percent confidence limits used herein indicate a 95-percent probability that the true mean of the test data lies within the limits. For material system I, G_{range} best correlates the data.

Material system II.- Figure 9(a) shows the debond-propagation rates for two specimen thicknesses tested at several stress ratios plotted against S_{max}. Again, for a given value of S_{max}, lower stress ratios and thicker specimens produced faster debonding.

Figures 9(b), (c), and (d) show these rates plotted against G_{max}, G_{range}, and $G_{max \cdot range}$. As for material system I, G_{range} correlates the data better than G_{max}. But, unlike material system I, $G_{max \cdot range}$ correlates the data better than G_{range} alone. In this case da/dN appears to be a function of both maximum load and load range.

Material system III.- Figure 10(a) shows the debond-propagation rates for material system III plotted against S_{max}. As with material systems I and II, lower stress ratios and thicker specimens produced faster debonding.

Figures 10(b), (c), and (d) show the rates correlated as before. The data are correlated best by $G_{max \cdot range}$, and da/dN appears to be a function of both maximum stress and stress range. But, in contrast to material systems I and II, G_{max} correlated the data better than G_{range}.

To summarize, for all three material systems an equation of the general form

$$G = \frac{t_1 t_2 E_1 w}{E_2\left(2t_1 E_1 + t_2 E_2\right)} \sigma^2$$

(which is eq. (16)) correlated the data quite well. However, the specific form of this equation that best correlated the data seemed to be material dependent. For material system I,

G_{range} best correlated the data; but for material systems II and III, $G_{max \cdot range}$ best correlated the data. The coefficients and exponents determined by fitting equation (24) to the test data, and the sum of residuals for all three material systems are shown in the following table:

Correlating parameters	Material system								
	I			II			III		
	c	n	Σr^2	c	n	Σr^2	c	n	Σr^2
G_{max}	5.94^{-14}	3.94	16.7	9.55^{-12}	1.81	0.48	2.61^{-15}	3.91	1.62
G_{range}	5.88^{-13}	3.73	5.59	6.13^{-10}	1.28	.18	6.31^{-12}	2.75	2.18
$G_{max \cdot range}$	4.83^{-14}	4.22	7.84	4.56^{-11}	1.72	.14	1.17^{-13}	3.40	1.09

Because the number of data points varied among the systems, Σr^2 for different systems should not be compared. The finding that different forms of G correlated the different material systems may be attributed to a number of factors: the assumed forms of the correlating parameters and of equation (24), the observed differences in failure mechanisms among the material systems, the assumed value of ΔT in material systems II and III, and so forth. Evidently the basic key parameters and functional forms are yet to be defined. Consequently, variations of best correlating parameters for different material systems are not surprising, and empirical correlating expressions applicable for one bonded system may not be appropriate for another system.

CONCLUDING REMARKS

Cyclic debonding rates were measured for room-temperature tests of three material systems: graphite/epoxy bonded to aluminum at room temperature, graphite/epoxy bonded to aluminum at an elevated temperature, and S-glass/epoxy bonded to aluminum at an elevated temperature. Loading in all tests was at constant amplitude. During each test, debonding was monitored with a photoelastic-coating technique. The rates of debonding were compared with three expressions based on strain-energy release rate in terms of the maximum stress, stress range, and a combination of the two.

The debond-propagation rates were significantly influenced by both adherend thickness and the cyclic stress ratio. For a given maximum stress, the thicker specimens debonded faster than the thinner ones, and the specimens tested at lower stress ratios debonded faster than specimens tested at higher stress ratios. Microscopic examinations of the debonded surfaces showed significantly different failure mechanisms for different

material systems. For graphite bonded to aluminum with a room-temperature-curing adhesive, failure occurred within the adhesive. For graphite bonded to aluminum with an elevated-temperature-curing adhesive, failure occurred primarily in the matrix near the adhesive interface. For S-glass bonded to aluminum with an elevated-temperature-curing adhesive, failure occurred primarily at the composite-adhesive interface.

The strain-energy release rate correlated the data quite well for each of the three material systems, but the form of the best correlating expression varied. Consequently, empirical correlating expressions applicable to one bonded system may not be appropriate for another bonded system, and caution should be exercised in drawing parallels between different material systems without supporting test data.

Langley Research Center
National Aeronautics and Space Administration
Hampton, Va. 23665
December 4, 1975

APPENDIX

DEVELOPMENT OF STRAIN-ENERGY RELEASE RATE EQUATION

The rate at which strain energy is released when a metal debonds from a composite (fig. 3) was given in the body of this paper (eq. (14)) as

$$G = P(\epsilon_A - \epsilon_C) - w\left[\phi_{A,2}t_2 - \left(\phi_{C,2}t_2 + 2\phi_{C,1}t_1\right)\right] \tag{A1}$$

In this appendix, the right-hand terms are evaluated to derive an explicit expression for G (eq. (15)). The strains in equation (A1) were defined by requiring equilibrium of forces, strain compatibility among the layers, and a constitutive relation between stress and strain in specimen regions A and C. Equilibrium is satisfied by

$$P = w\int \sigma\, dy \tag{A2}$$

For the one-dimensional analysis used in this problem, strain compatibility was assured by assuming that the strain through the specimen thickness was constant. The constitutive relation for the problem is given as (ref. 6, p. 259)

$$\sigma = E(\epsilon - \alpha\,\Delta T) \tag{A3}$$

These three relationships are used to calculate the strains, strain-energy density, and strain-energy release rate in regions A and C, as shown in the equations that follow.

In region A, equilibrium is satisfied when

$$P = St_2w = \sigma_{A,2}t_2w \tag{A4}$$

The constitutive equation (A3) for region A is

$$\sigma_{A,2} = E_2(\epsilon_A - \alpha_2\,\Delta T) \tag{A5}$$

Substituting equation (A5) into equation (A4) and solving for ϵ_A yield

$$\epsilon_A = \frac{S}{E_2} + \alpha_2\,\Delta T \tag{A6}$$

In region C, compatibility is satisfied when

$$\epsilon_{C,1} = \epsilon_{C,2} = \epsilon_C \tag{A7}$$

APPENDIX

Equilibrium in region C is satisfied when

$$P = St_2w = 2t_1w\sigma_{C,1} + \sigma_{C,2}t_2w \tag{A8}$$

The constitutive relationships in region C for the metal and composite, respectively, are

$$\sigma_{C,1} = E_1(\epsilon_C - \alpha_1 \Delta T) \tag{A9}$$

$$\sigma_{C,2} = E_2(\epsilon_C - \alpha_2 \Delta T) \tag{A10}$$

Substituting equations (A9) and (A10) into equation (A8) and solving for ϵ_C lead to

$$\epsilon_C = \frac{St_2 + \Delta T(2E_1t_1\alpha_1 + E_2t_2\alpha_2)}{2E_1t_1 + E_2t_2} \tag{A11}$$

The strain-energy density can be expressed as

$$\phi = \frac{\sigma^2}{2E} = \frac{[E(\epsilon - \alpha \Delta T)]^2}{2E} \tag{A12a}$$

or

$$\phi = \frac{E}{2}[\epsilon^2 - 2\epsilon\alpha \Delta T + \alpha^2(\Delta T)^2] \tag{A12b}$$

For region A, substituting equation (A6) into equation (A12b) yields

$$\phi_{A,2} = \frac{E_2}{2}[\epsilon_A{}^2 - 2\epsilon_A\alpha_2 \Delta T + \alpha_2{}^2(\Delta T)^2] \tag{A13}$$

Similarly, for region C, substitution of equation (A11) into equation (A12b) yields for the metal

$$\phi_{C,1} = \frac{E_1}{2}[\epsilon_C{}^2 - 2\epsilon_C\alpha_1 \Delta T + \alpha_1{}^2(\Delta T)^2] \tag{A14}$$

and for the composite

$$\phi_{C,2} = \frac{E_2}{2}[\epsilon_C{}^2 - 2\epsilon_C\alpha_2 \Delta T + \alpha_2{}^2(\Delta T)^2] \tag{A15}$$

APPENDIX

Substitution of equations (A6), (A8), (A11), (A13), (A14), and (A15) into equation (A1) yields

$$G = \frac{t_1 t_2 E_1 w}{E_2\left(2t_1 E_1 + t_2 E_2\right)}\left[S - \Delta T(\alpha_1 - \alpha_2)E_2\right]^2 \tag{A16}$$

the desired expression for strain-energy release rate (eq. (15)).

REFERENCES

1. Johnson, R. W.; and June, R. R.: Application Study of Filamentary Composites in a Commercial Jet Aircraft Fuselage. NASA CR-112110, 1972.

2. Blichfeldt, B.; and McCarty, J. E.: Analytical and Experimental Investigation of Aircraft Metal Structures Reinforced With Filamentary Composites. Phase II – Structural Fatigue, Thermal Cycling, Creep, and Residual Strength. NASA CR-2039, 1972.

3. Mechtly, E. A.: The International System of Units – Physical Constants and Conversion Factors (Second Revision). NASA SP-7012, 1973.

4. Paris, Paul C.; and Sih, George C.: Stress Analysis of Cracks. Fracture Toughness Testing and Its Applications, Spec. Tech. Publ. No. 381, American Soc. Testing & Mater., c.1965, pp. 30-83.

5. Draper, N. R.; and Smith, H.: Applied Regression Analysis. John Wiley & Sons, Inc., c.1966.

6. Boley, Bruno A.; and Weiner, Jerome H.: Theory of Thermal Stresses. John Wiley & Sons, Inc., c.1960.

TABLE I.- MATERIAL PROPERTIES

Material	Modulus of elasticity, E, GPa	Thermal coefficient of expansion, α, μK^{-1}
7075-T6 aluminum alloy	71	22.50
Graphite/epoxy	131	-.38
S-glass/epoxy	61	3.60

TABLE II.- RESULTS OF CYCLIC DEBONDING TESTS ON MATERIAL SYSTEM I
(ALUMINUM AND GRAPHITE/EPOXY, EA-927R ADHESIVE CURED AT RT)

Thickness		R	S_{max}, MPa	da/dN, μm/cycle	G_{max}, J/m	G_{range}, J/m	$G_{max \cdot range}$, J/m
t_1, mm	t_2, mm		(a)	(b)	(c)	(d)	(e)
0.51	0.84	0.10	485	0.000714	15	12	14
↓	.79	.10	722	.0920	33	27	30
	.81	.10	804	.146	41	33	37
↓	.81	.10	1206	2.50	93	75	83
1.02	1.68	.34	431	.00318	24	10	16
↓	1.60	.10	438	.0168	24	20	22
	1.78	.21	468	.0268	29	18	23
	1.63	.10	479	.0229	29	24	26
	1.65	.42	493	.00152	31	11	18
	1.63	.42	495	.00190	31	10	18
	1.85	.29	518	.127	36	18	26
	1.85	.48	528	.00927	38	10	20
	1.63	.10	532	.166	36	29	32
	1.70	.01	572	.335	42	42	42
	1.73	.19	577	.373	44	29	35
	1.68	.10	578	.373	43	35	39
	1.75	.36	586	.0589	45	18	29
	1.91	.18	656	1.03	58	39	48
	1.60	.10	657	.498	55	44	49
	1.68	.10	683	1.32	60	49	54
↓	1.60	.10	766	1.78	74	60	67
1.60	2.41	.10	219	.00689	9	8	8
↓	2.51	.10	269	.0315	14	12	13
	2.51	.10	322	.0569	21	17	19
	2.34	.42	343	.000678	23	8	13
	2.49	.10	377	.00785	28	23	25
	2.52	.24	381	.00424	29	17	22
	2.49	.10	431	.163	37	30	33
	2.46	.34	447	.0866	39	17	26
	2.44	.21	495	.254	48	30	38
	2.46	.42	505	.0290	50	8	29
	2.54	.10	535	1.32	57	46	51
	2.39	.29	559	.399	61	31	43
	2.54	.10	589	5.59	69	56	62
	2.39	.01	596	4.52	69	68	69
↓	2.34	.19	614	3.18	73	48	59

[a]Stress in composite in region A.
[b]Calculated from linear portion of debond length vs cycles curve.
[c]Calculated using σ_{max}.
[d]Calculated using $\sigma_{max} - \sigma_{min}$.
[e]Calculated using σ_{max} and $\sigma_{max} - \sigma_{min}$.

TABLE III.- RESULTS OF CYCLIC DEBONDING TESTS ON MATERIAL SYSTEM II

(ALUMINUM AND GRAPHITE/EPOXY, AF-126 ADHESIVE CURED AT 394 K)

Thickness		R	S_{max}, MPa	da/dN μm/cycle	G_{max}, J/m	G_{range}, J/m	$G_{max \cdot range}$, J/m
t_1, mm	t_2, mm		(a)	(b)	(c)	(d)	(e)
1.02	1.65	0.10	371	0.0150	58	14	29
	1.65	.10	424	.0193	67	19	35
	1.57	.10	542	.0302	89	30	52
	1.63	.30	548	.0226	92	19	42
	1.57	.30	552	.0294	91	19	41
	1.57	.30	552	.0306	91	19	41
	1.63	.10	585	.0635	100	35	59
	1.65	.10	638	.0592	113	42	69
	1.63	.10	692	.112	126	49	79
	1.57	.10	704	.0899	127	51	80
1.60	2.59	.10	318	.0279	77	17	36
	2.46	.10	434	.0437	106	30	57
	2.62	.10	475	.0627	122	37	67
	2.51	.10	484	.0650	122	38	68
	2.54	.10	535	.0734	139	46	80
	2.39	.42	549	.0254	146	21	55
	2.62	.42	549	.0508	141	20	53
	2.54	.10	588	.116	158	56	94
	2.46	.10	652	.144	178	68	110

[a]Stress in composite in region A.

[b]Calculated from linear portion of debond length vs cycles curve.

[c]Calculated using σ_{max}.

[d]Calculated using $\sigma_{max} - \sigma_{min}$.

[e]Calculated using σ_{max} and $\sigma_{max} - \sigma_{min}$.

TABLE IV.- RESULTS OF CYCLIC DEBONDING TESTS ON MATERIAL SYSTEM III

(ALUMINUM AND S-GLASS/EPOXY, AF-126 ADHESIVE CURED AT 394 K)

Thickness		R	S_{max}, MPa	da/dN, μm/cycle	G_{max}, J/m	G_{range}, J/m	$G_{max \cdot range}$, J/m
t_1, mm	t_2, mm		(a)	(b)	(c)	(d)	(e)
1.02	0.89	0.10	324	0.0305	52	23	35
	.89	.10	379	.0607	66	31	45
	.89	.10	433	.0772	81	41	58
	.86	.34	453	.0419	82	23	43
	.91	.10	482	.187	97	51	71
	.86	.21	495	.0886	98	40	63
	.89	.42	502	.0435	103	23	49
	.89	.10	541	.409	116	64	86
	.86	.29	555	.250	118	41	69
	.86	.01	592	.826	132	91	109
	.89	.10	595	.605	136	77	103
	.86	.19	603	.419	136	63	92
	.86	.36	614	.199	140	41	75
	.89	.10	650	1.26	158	92	120
	.86	.26	664	.465	160	63	101
	.89	.10	704	2.03	181	108	140
	.86	.18	712	1.11	180	90	127
	.89	.10	757	2.95	205	125	160
1.60	1.40	.10	218	.0078	47	16	28
	1.42	.10	269	.0254	63	25	40
	1.42	.10	323	.0838	82	36	54
	1.45	.10	370	.181	102	48	70
	1.37	.29	411	.437	116	36	64
	1.42	.10	432	.546	128	65	91
	1.37	.35	443	.648	130	35	67
	1.42	.22	472	1.13	148	58	92
	1.42	.10	484	1.14	154	81	112
	1.42	.04	511	3.48	168	103	131
	1.42	.10	538	1.85	183	100	135
	1.40	.29	538	1.61	181	62	106
	1.40	.10	540	3.07	182	100	135
	1.40	.18	592	3.68	212	100	145
	1.37	.10	606	3.33	217	124	164
	1.45	.10	634	5.92	244	142	186

[a]Stress in composite in region A.

[b]Calculated from linear portion of debond length vs cycles curve.

[c]Calculated using σ_{max}.

[d]Calculated using $\sigma_{max} - \sigma_{min}$.

[e]Calculated using σ_{max} and $\sigma_{max} - \sigma_{min}$.

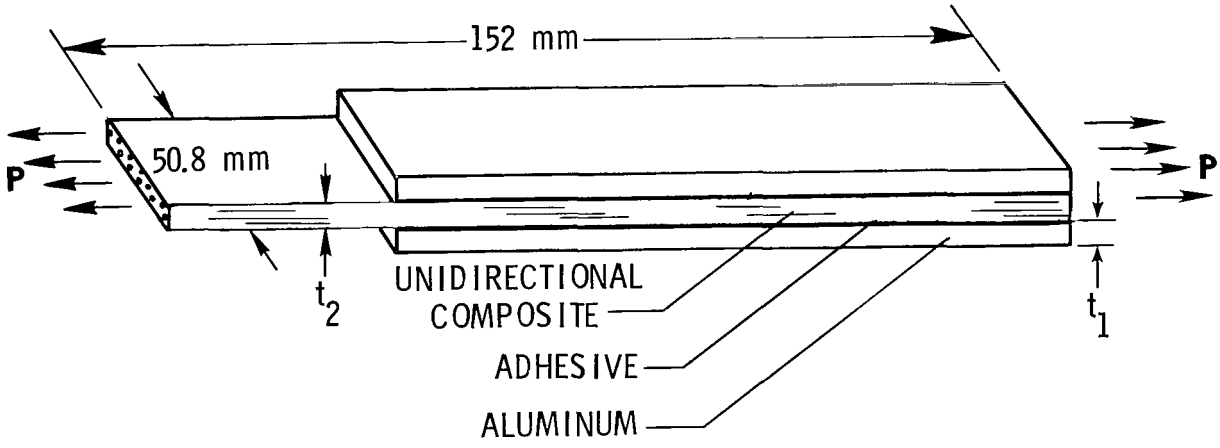

Figure 1.- Specimen configuration.

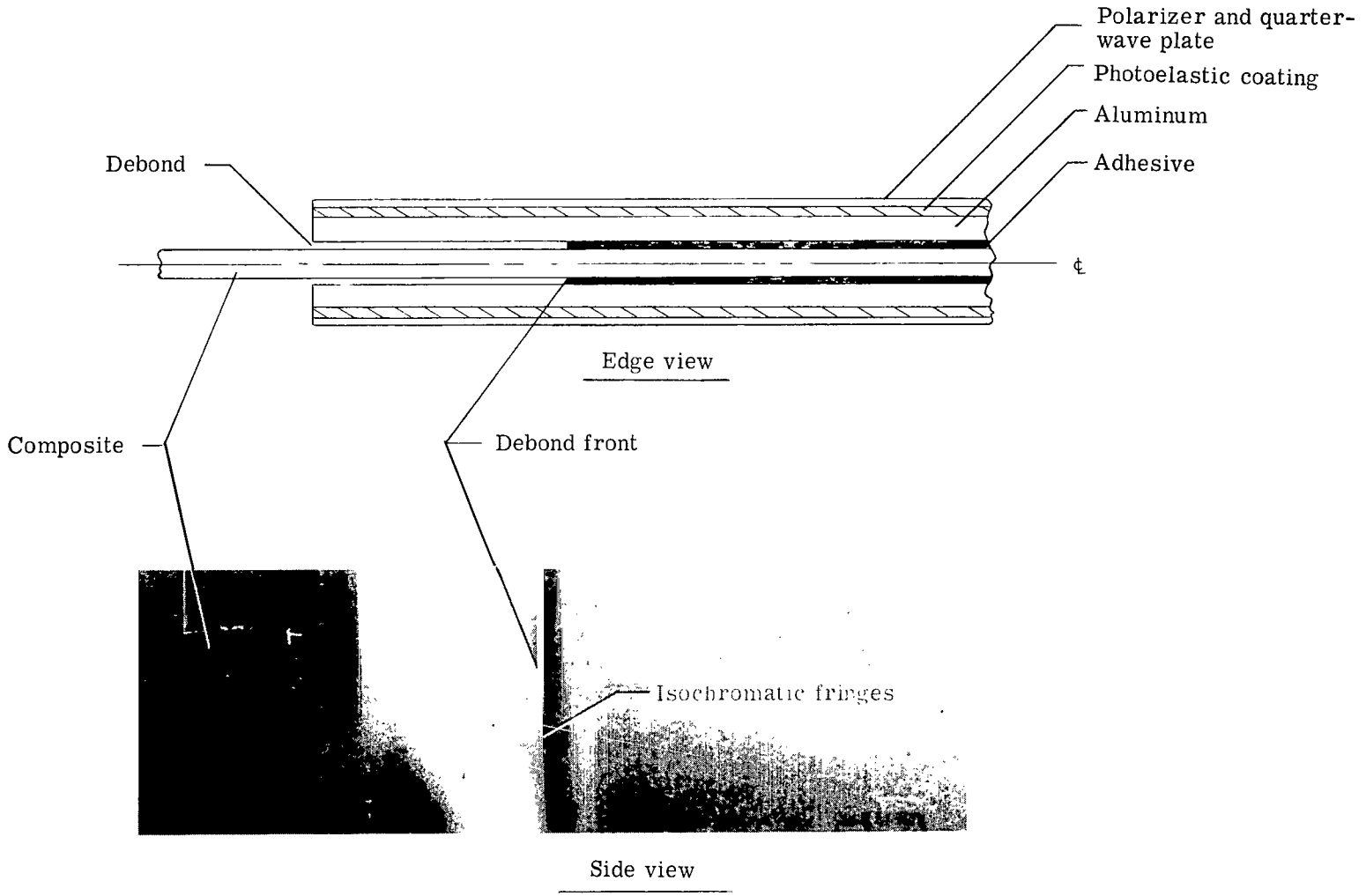

Figure 2.- Partially debonded specimen.

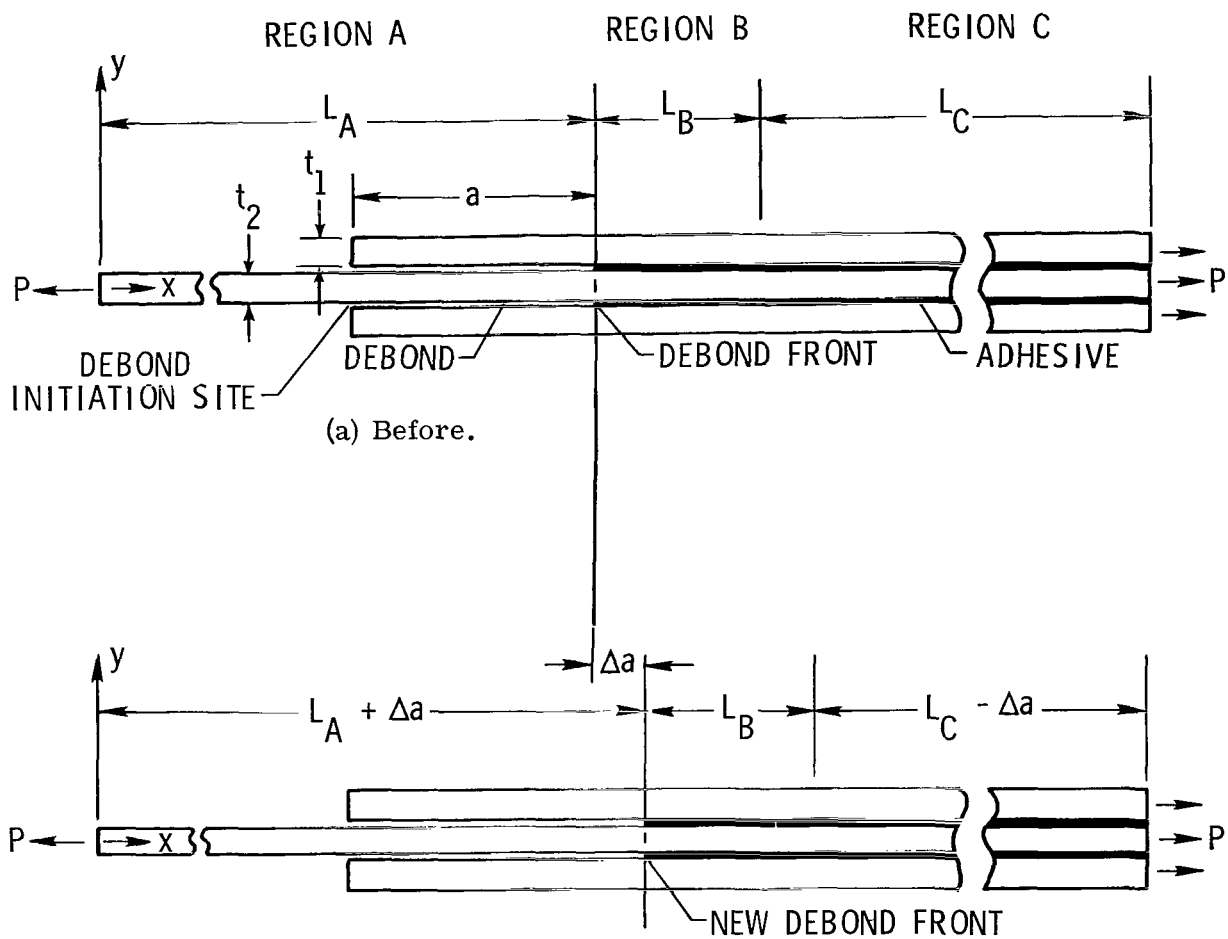

Figure 3.- Test specimen before and after an increment of debonding Δa.

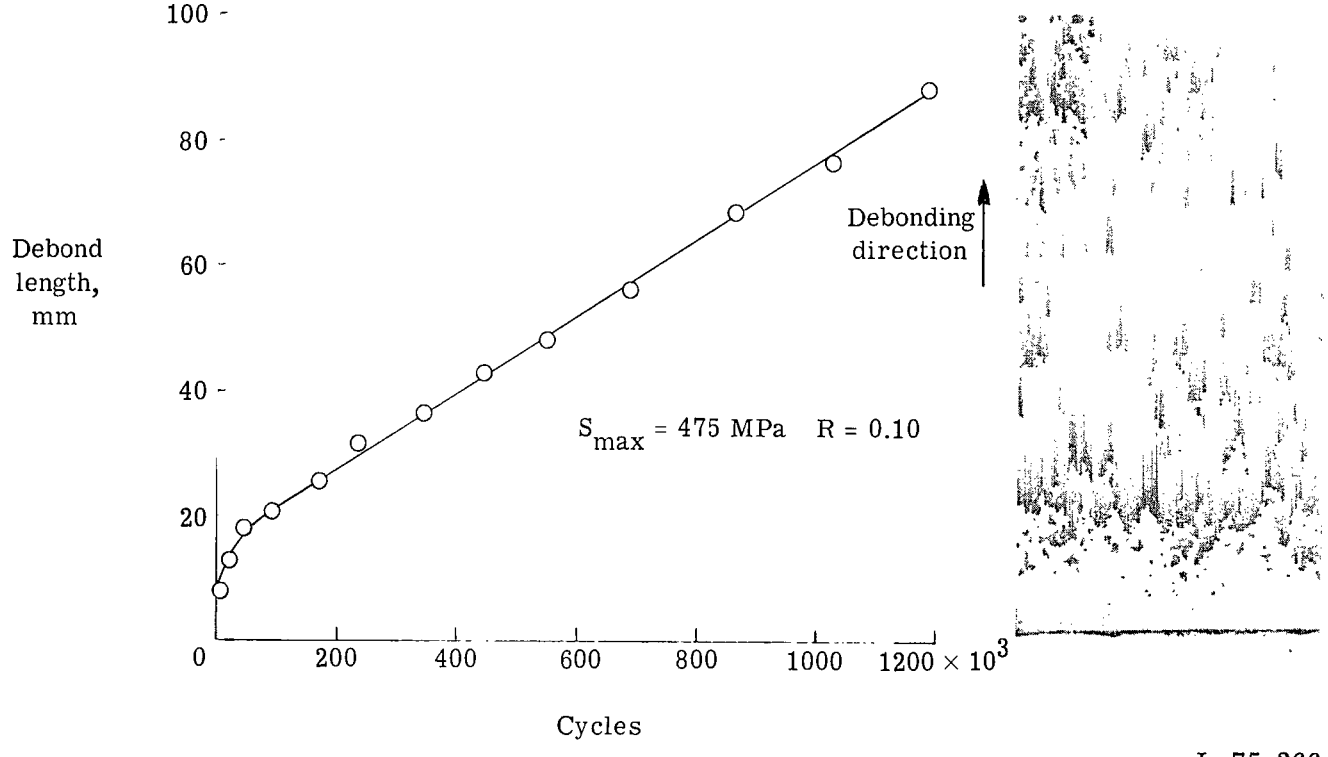

Figure 4.- Typical variation of debond length with cycles. (Example is for an aluminum and graphite/epoxy specimen with AF-126 adhesive cured at 394 K; material system II.)

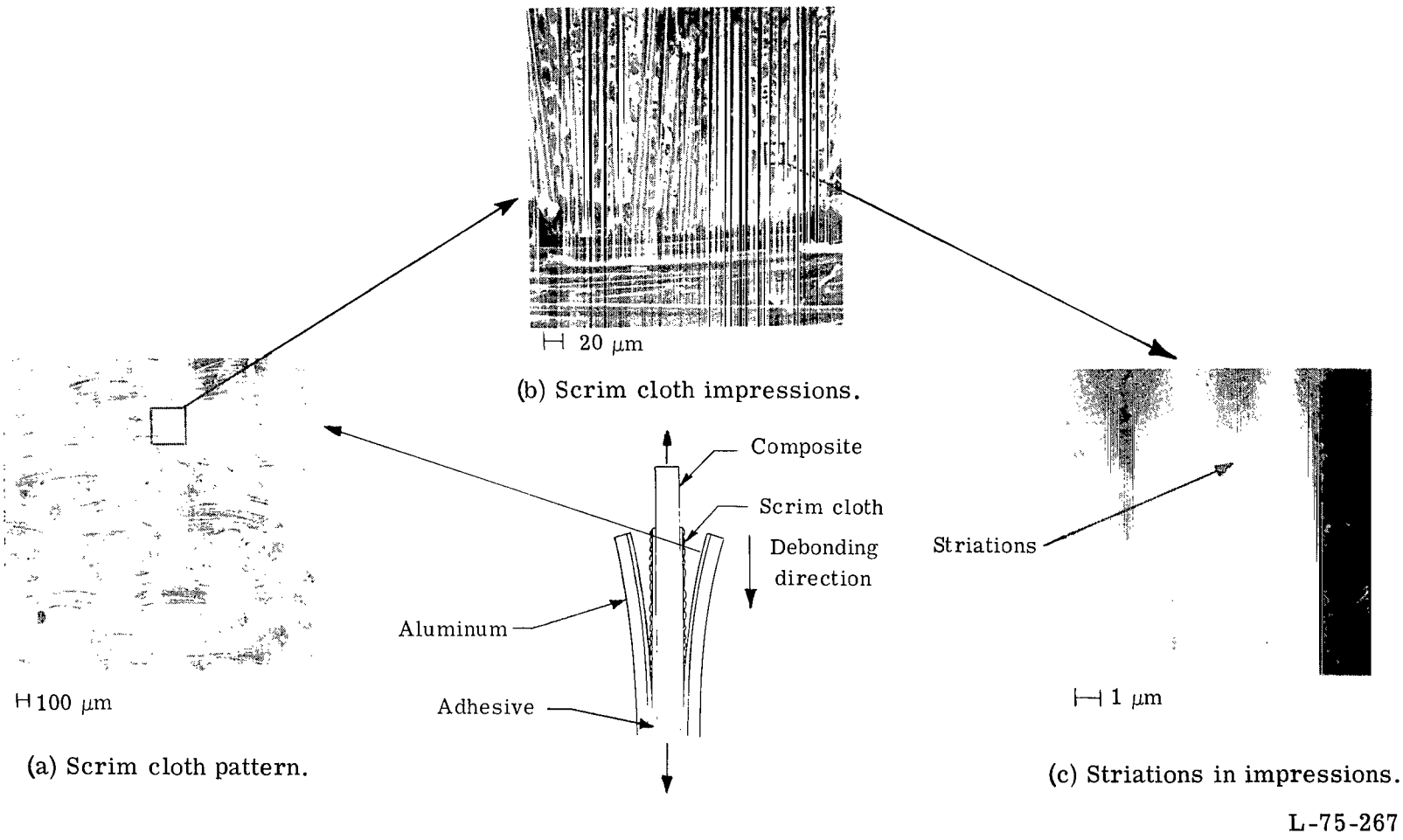

Figure 5.- Failure surface of graphite/epoxy and aluminum specimen with EA-927R adhesive cured at RT. Material system I.

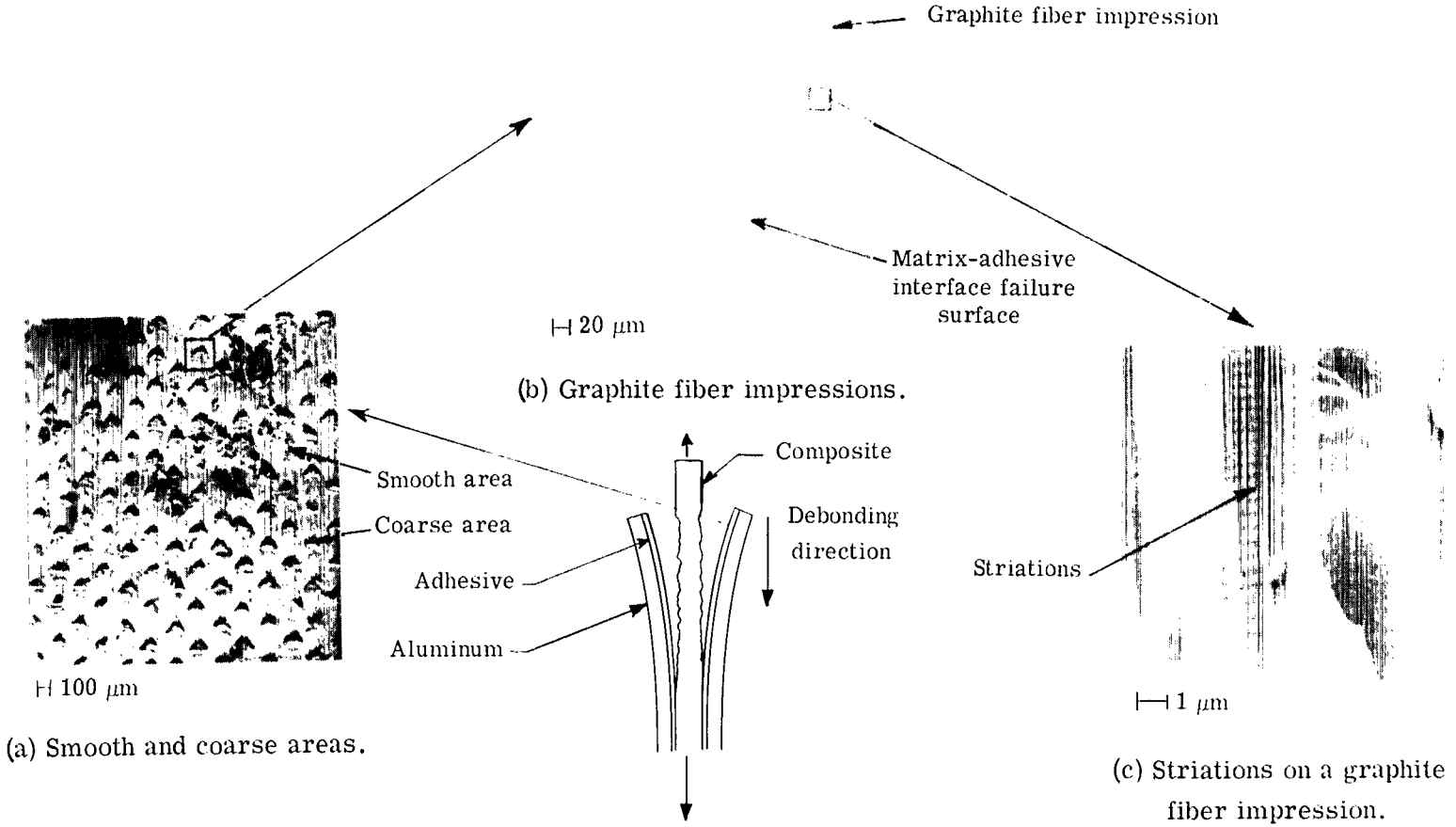

Figure 6.- Failure surface of graphite/epoxy and aluminum specimen with AF-126 adhesive cured at 394 K. Material system II.

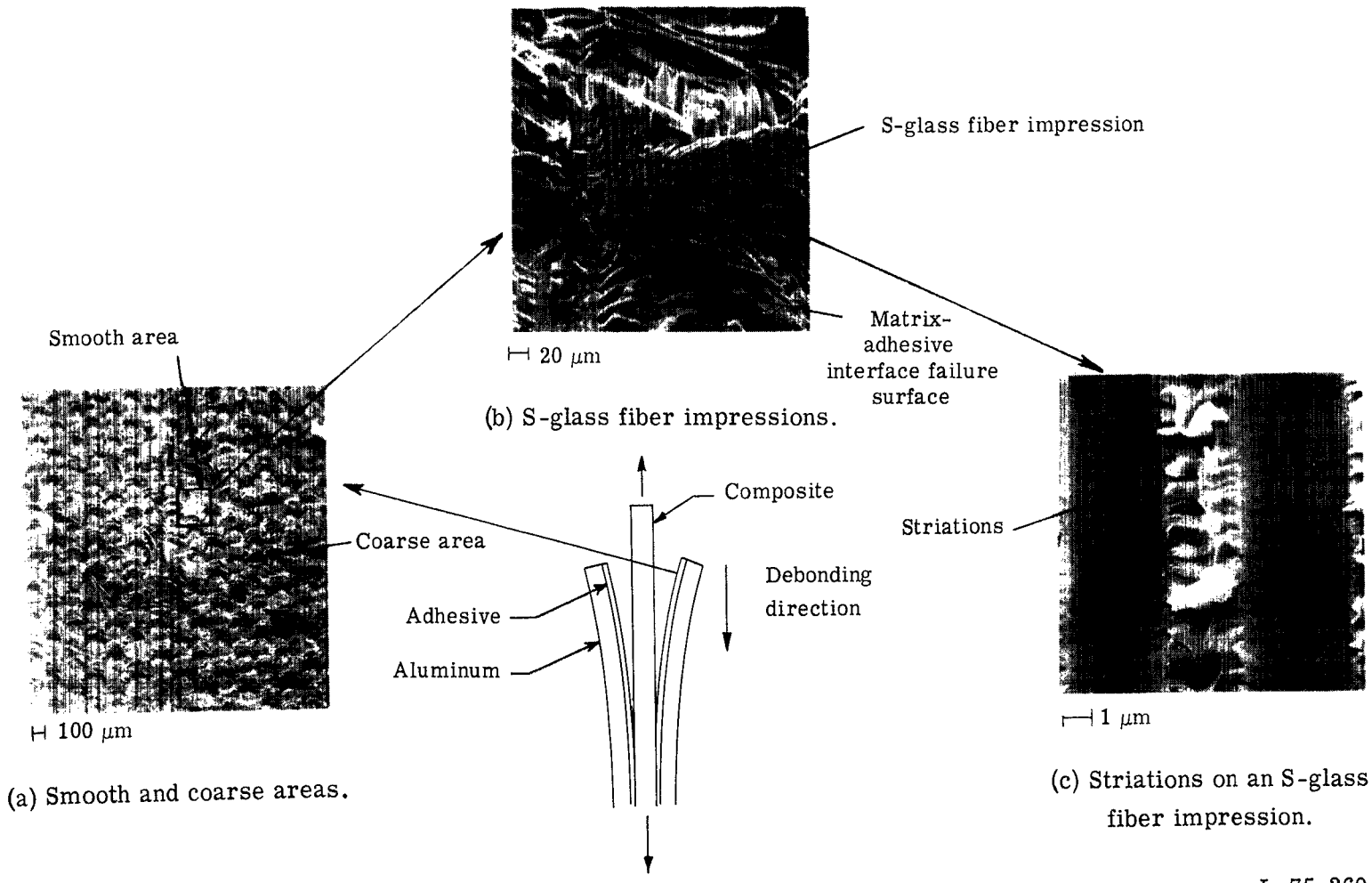

Figure 7.- Failure surface of S-glass/epoxy and aluminum specimen with AF-126 adhesive cured at 394 K. Material system III.

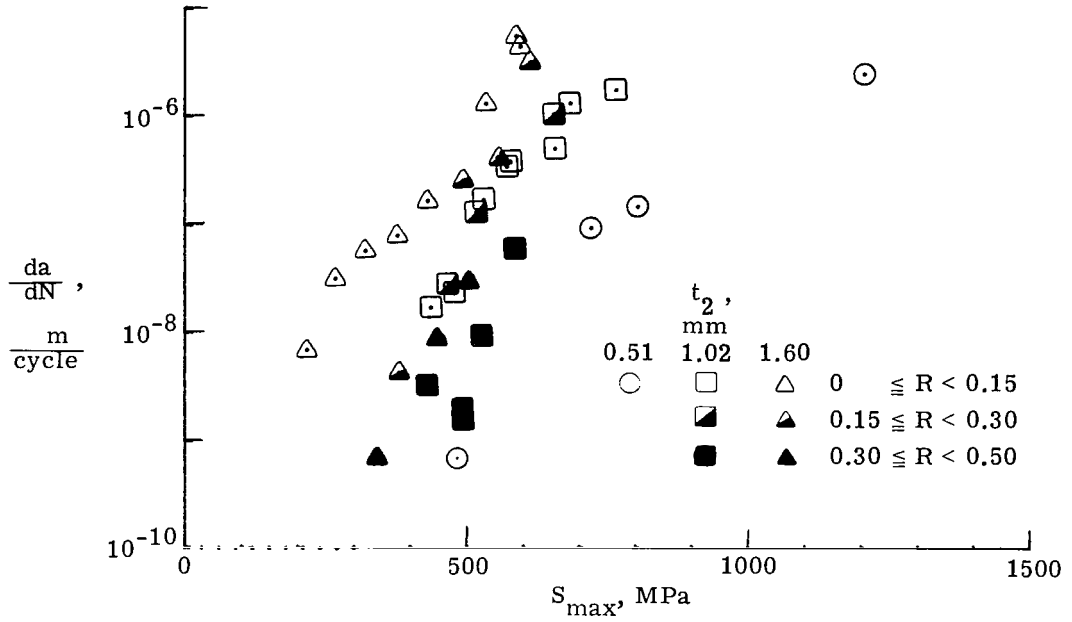

(a) da/dN against S_{max}.

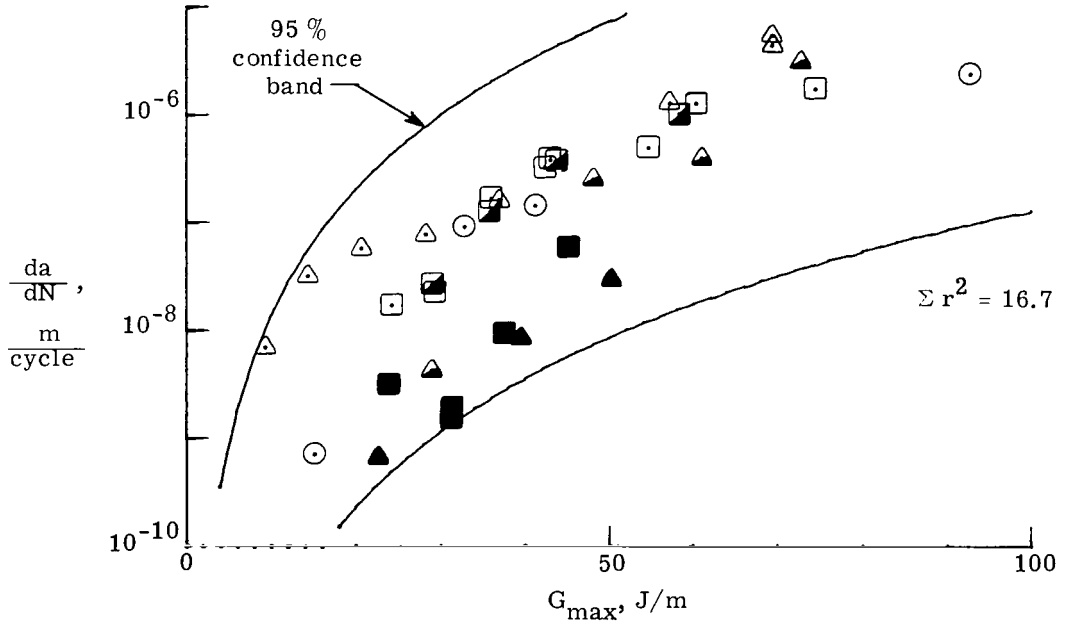

(b) da/dN against G_{max}.

Figure 8.- Correlation parameters for debond-propagation rate for aluminum and graphite/epoxy specimen with EA-927R adhesive cured at RT. Material system I.

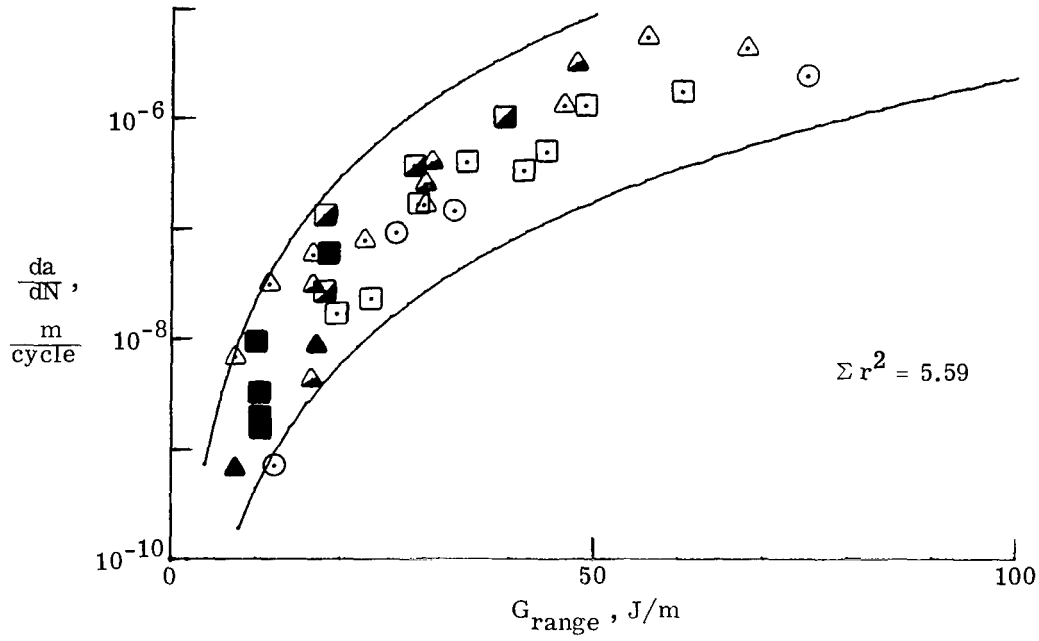

(c) da/dN against G_{range}.

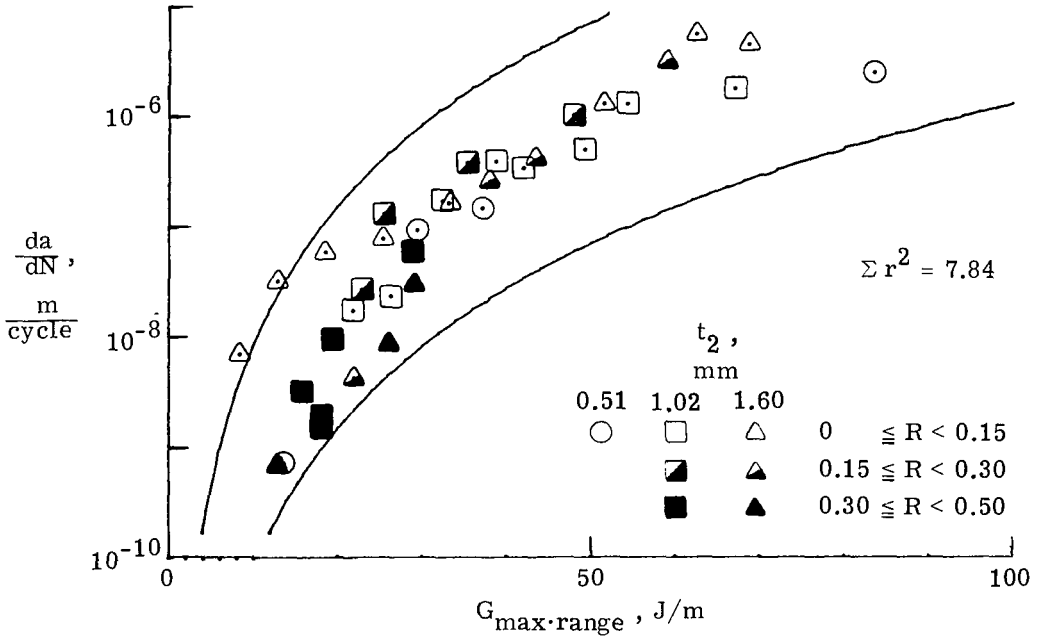

(d) da/dN against $G_{max \cdot range}$.

Figure 8.- Concluded.

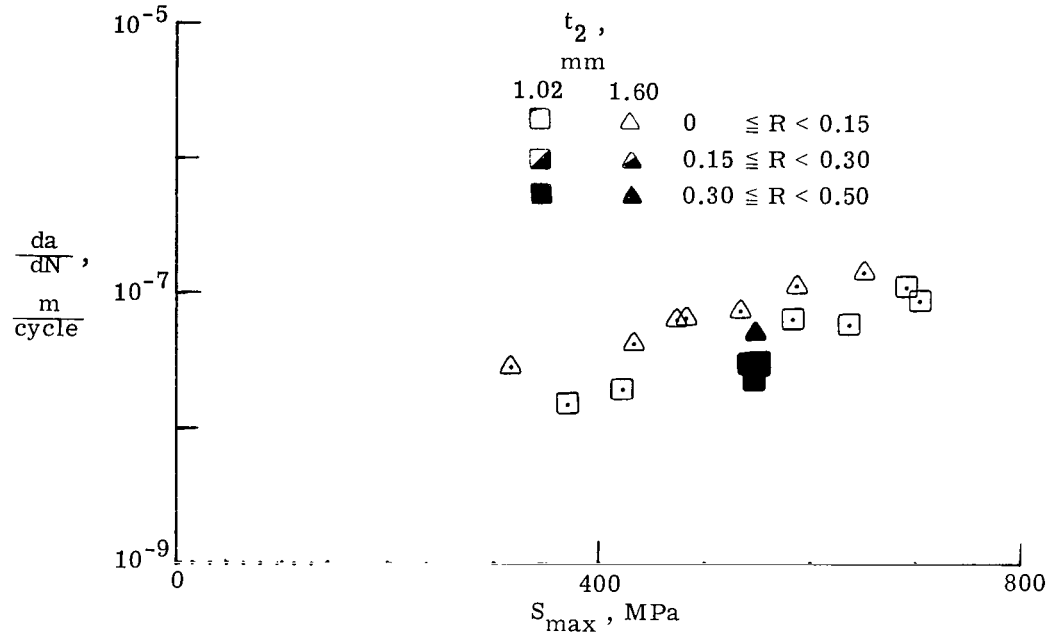

(a) da/dN against S_{max}.

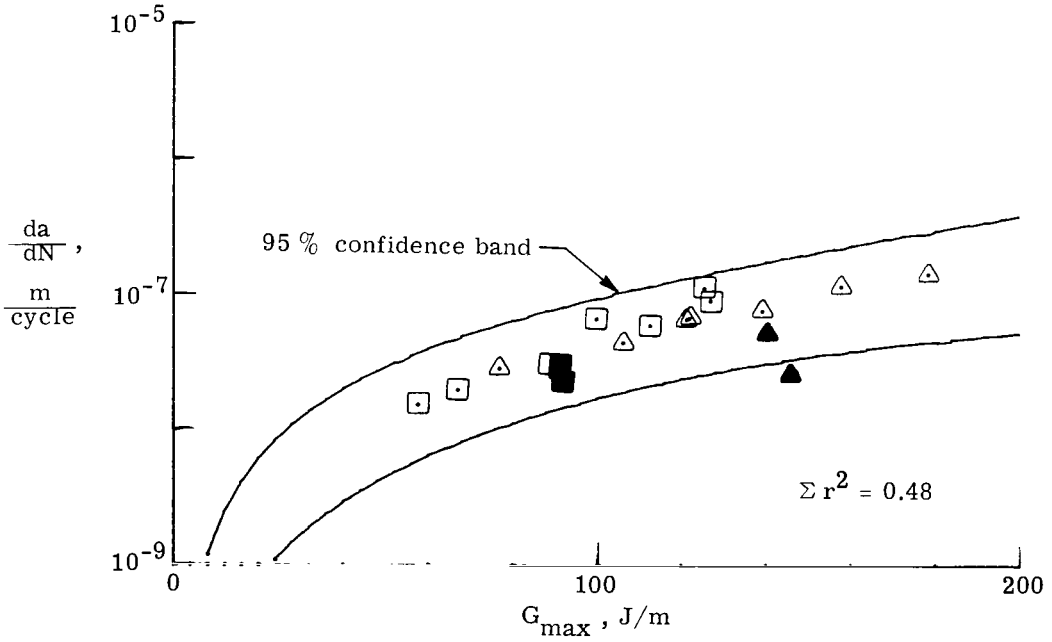

(b) da/dN against G_{max}.

Figure 9.- Correlation parameters for debond-propagation rate for aluminum and graphite/epoxy specimen with AF-126 adhesive cured at 394 K. Material system II.

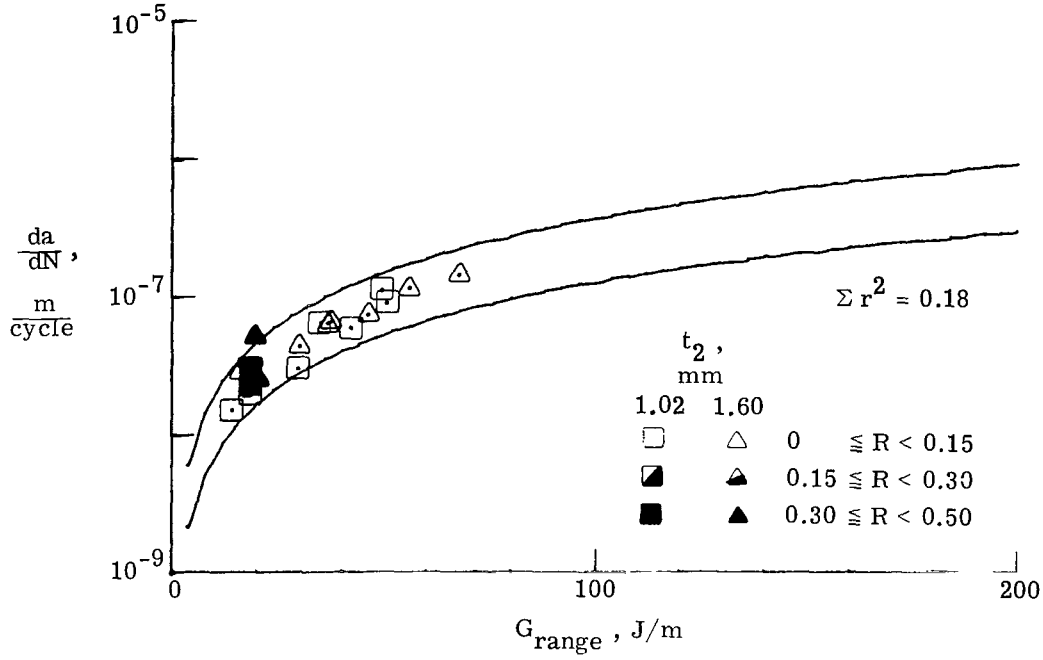

(c) da/dN against G_{range}.

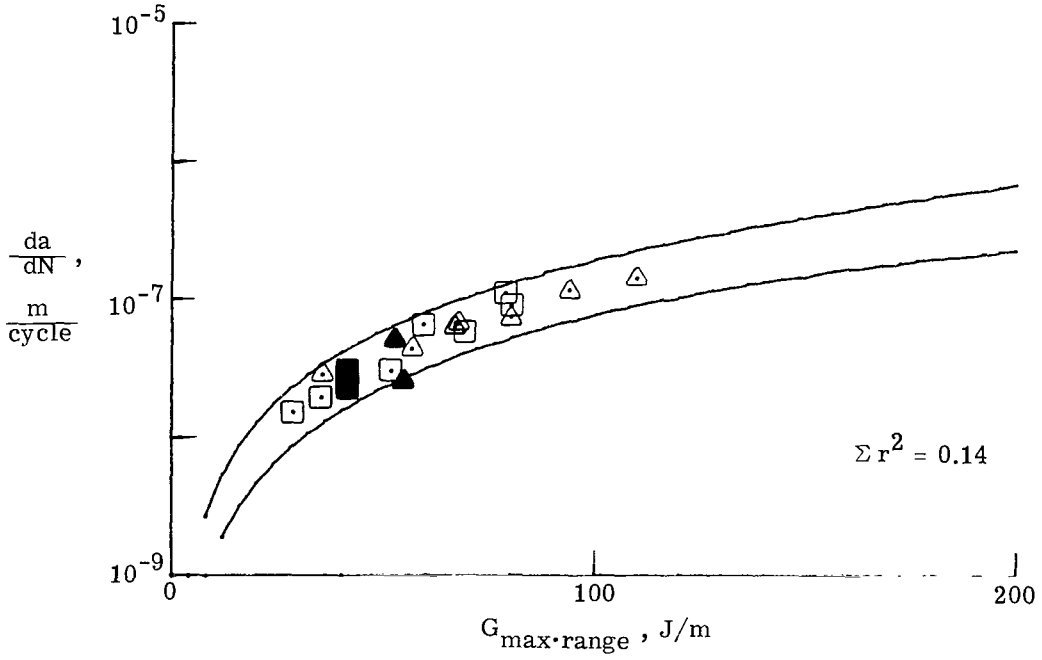

(d) da/dN against $G_{max\cdot range}$.

Figure 9.- Concluded.

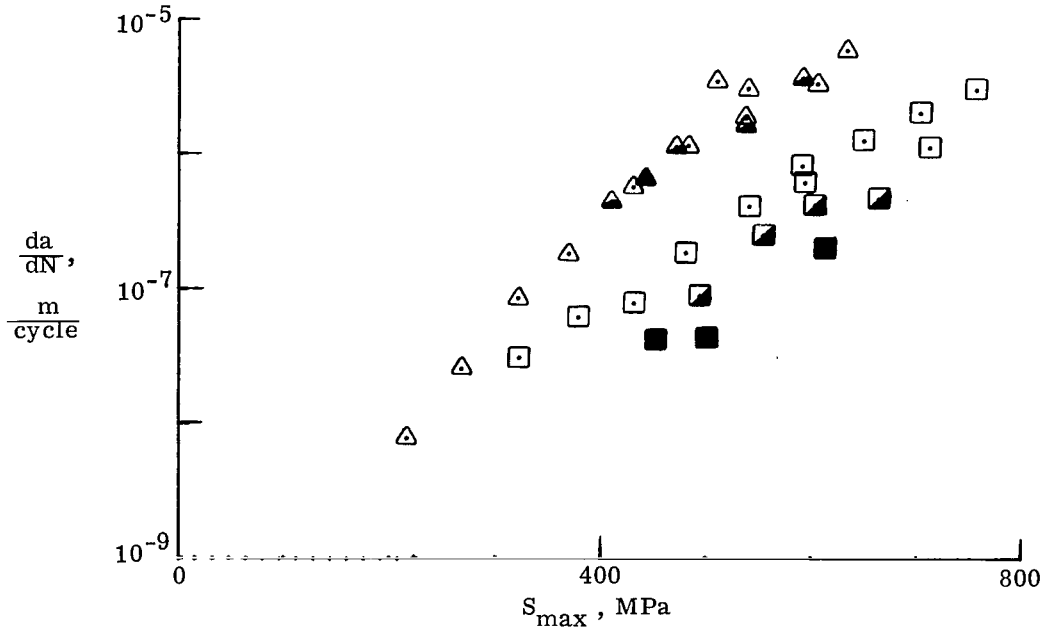

(a) da/dN against S_{max}.

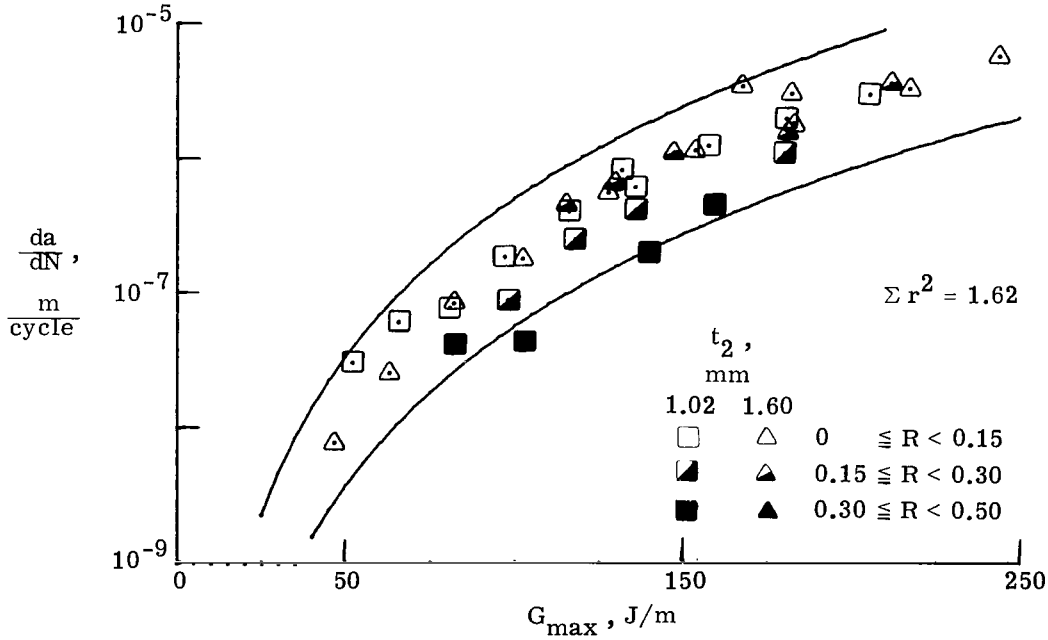

(b) da/dN against G_{max}.

Figure 10.- Correlation parameters for debond-propagation rate for aluminum and S-glass/epoxy specimen with AF-126 adhesive cured at 394 K. Material system III.

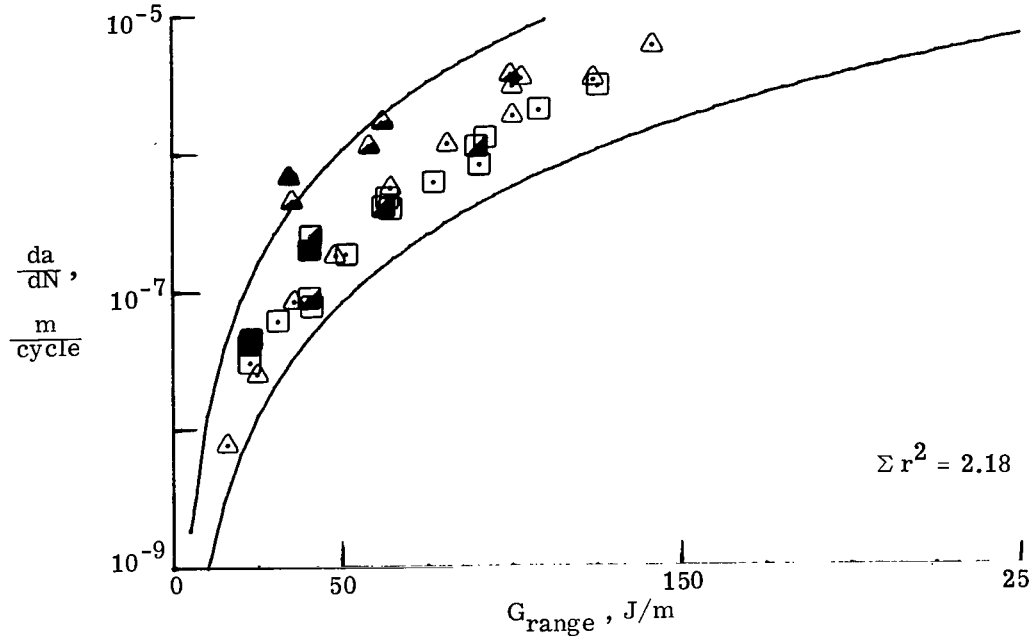

(c) da/dN against G_{range}.

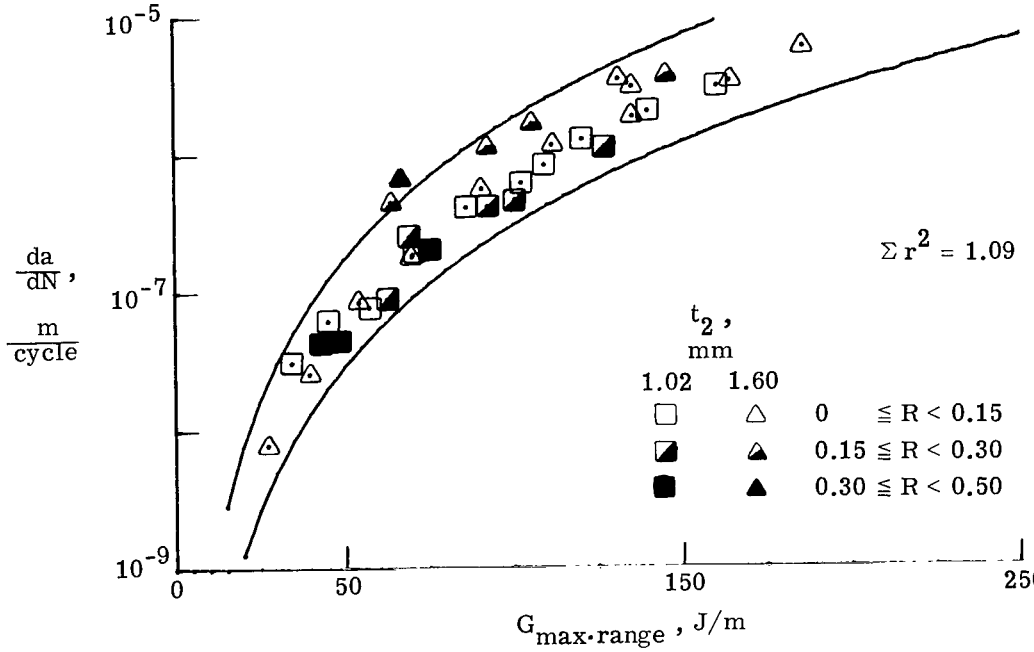

(d) da/dN against $G_{max\cdot range}$.

Figure 10.- Concluded.